NETmix®, a New Type of Static Mixer: Experimental Characterization and Model Validation

Paulo E. Laranjeira and António A. Martins
Laboratory of Separation and Reaction Engineering, Departamento de Engenharia Química, Faculdade de Engenharia da Universidade do Porto, Rua Dr. Roberto Frias, 4200-465 Porto, Portugal

Maria Isabel Nunes
Centre for Environmental and Marine Studies (CESAM), Departamento de Ambiente e Planeamento, Universidade de Aveiro, Campus Universitário de Santiago, 3810-193 Aveiro, Portugal

José Carlos B. Lopes and Madalena M. Dias
Laboratory of Separation and Reaction Engineering, Departamento de Engenharia Química, Faculdade de Engenharia da Universidade do Porto, Rua Dr. Roberto Frias, 4200-465 Porto, Portugal

DOI 10.1002/aic.12316
Published online June 25, 2010 in Wiley Online Library (wileyonlinelibrary.com).

In a previous article (Laranjeira et al.), a network model was developed to describe and predict the behavior and performance of NETmix®, a new type of static mixer consisting of a network of interconnected chambers and channels. This work reports experimental results on a transparent prototype NETmix® unit constructed to enable the characterization of the mixing mechanisms at the local scale. Tracer flow visualization experiments show that the mixing characteristics in the NETmix® unit depend on the Reynolds number both for macromixing and micromixing. A critical Reynolds number for the onset of mixing was obtained where oscillating flow in the chambers is observed. Chemical reaction experiments were done using test reactions systems that exhibit mixing effects in the final product distribution and selectivity. Reaction selectivity was shown to depend on the reactants injection scheme. Theoretical predictions obtained with the network model were in agreement with experimental data for high Reynolds numbers. © 2010 American Institute of Chemical Engineers *AIChE J,* 57: 1020–1032, 2011

Keywords: novel reactor, static mixing, network model, mixing

Introduction

In many chemical processes, the interplay between mixing and chemical reaction is of fundamental importance to the overall process performance. The design and operation of most chemical reactors and downstream separation units is intimately linked to how the reactant chemicals mix and react. For example, just the manner in which initially segregated reactants are brought together into the reactor can have a great impact on the evolution of the path of chemical products, particularly for fast reaction schemes.[1,2] Inefficient mixing usually has a deleterious effect on both the yield and the selectivity of reaction, by reducing the formation of desired products and enhancing the generation of undesired materials. This aspect is crucial when unwanted products must be separated in downstream processes, as the cost and

Correspondence concerning this article should be addressed to M. M. Dias at dias@fe.up.pt.

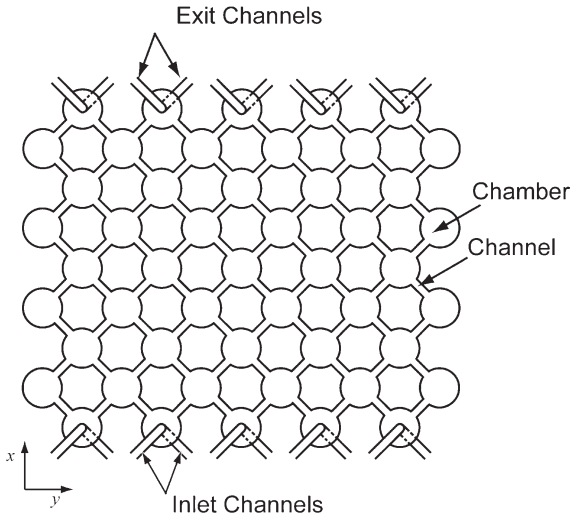

Figure 1. Schematic representation of a network of chambers and channels with $n_x = 4$ and $n_y = 5$.

dimensioning of such separation processes is directly related with the amount of undesired products present.[2,3] The availability of a model suitable to describe mixing and chemical reaction on a static mixer enables the maximization of the yield of the desired product, thus minimizing the costs of downstream separation processes and even upstream processing costs.

The NETmix® technology concept has been described in a previous publication,[4] based on a new static mixer consisting of a regular network of spherical chambers interconnected by cylindrical channels, as shown in Figure 1. To describe the mixing and reaction phenomena inside this novel mixer, a NETmix® model was developed where the chambers are modeled as perfectly mixed stirred tanks and the channels as perfect segregation plug flow devices. In this model, mixing quality is characterized by introducing a segregation parameter, α, defined as the ratio between the channels volume and the whole network volume. The network structure, with multiple entry points, enables the injection of reactants using different injection schemes, ranging from complete premixing to full segregation. The results have shown that both macromixing and micromixing characteristics can be programed and controlled, depending on the number of chamber rows in the direction of flow, the network segregation parameter, and the reactants injection scheme. Simulations with competitive second-order reactions have shown strong product distribution dependency on those parameters, and that under certain injection schemes, the NETmix® reactor leads to predicted selectivity values above those obtained in classical type of reactors. Furthermore, results from CFD simulations[5] have shown that above a critical channel Reynolds number, the flow field within each chamber strongly oscillates with typical well-defined frequencies inducing strong flow field dynamics that promote convective mixing with high efficiencies.

The objective of this work is to study chemical reaction in a network of chambers and channels with the NETmix® structure and validate the NETmix® model results. A NETmix® prototype experimental unit was designed and constructed and is described in detail in this work. Predictions of the NETmix® model are compared with experimental data to assess its validity and range of application using the following techniques: tracer and reaction visualization experiments and macromixing and micromixing assessment using a consecutive/competitive test reaction system.

Direct visualization of the flow and mixing studies in models and micromodel systems similar to NETmix® can be found in the literature, dealing mainly with the characterization of porous media, either single or multiphase flows. Micromodels and image analysis were used by Lanning and Ford[6] in their study of the bacterial dispersion in a network capillaries with a regular structure, and Corapcioglu and Ferdirchuck[7] studied the dispersion of a solute in a 2D system packed with a monolayer of spheres. Willingham et al.[8] used the same techniques to study the effects of the porous media structure and compare the experimental results and numerical predictions for a micromodel made by etching and with a variety of different structures. Other works used micromodels and direct visualization to study other phenomena in porous media, including the movement and dissolution of nonaqueous pollutants in porous media,[9–12] evolution of biomass development and propagation in a porous medium,[13–15] two-phase flow,[16] bubble growth in porous media,[17] and the comparison between Newtonian and non-Newtonian flow.[18] Zerai et al.[19] have used particle image velocimetry (PIV) to visualize the fluid flow in a chamber of a network with a geometrical structure similar to the NETmix® model, but no attempt to study the influence of the flow conditions and geometrical characteristics is included. Dertinger et al.[20] have considered microfluidic networks to generate complex concentration profiles, showing that diverse exit concentrations profiles can be obtained changing the way different dyes are introduced in the network and how its elements are organized.

Test reactions sensitive to mixing have been used to assess the performance of chemical reactors. Extensive reviews of the available test reactions sets proposed in the literature, kinetic constants, and other relevant aspects can be found in the literature.[21,22] Although static mixers feature high rates of energy dissipation and have short residence times, which are useful characteristics for reactions needing fast mixing to obtain high selectivity,[23] very few experimental studies of micromixing in static mixers can be found in the literature. Meyer et al.[24] assessed micromixing in a static mixer and in an empty tube by characterizing the product distribution of barium sulfate-EDTA complex in alkaline medium under the influence of an acid. Experiments were carried out in the range of Reynolds numbers $0.4 < Re < 300$ by varying the fluid viscosity and the flow rate. Bourne and Maire[25] determined the mixing intensity of three static mixers, differing mainly in the width of their channels, by applying the engulfment model[26,27] to the measured product distribution of fast consecutive competitive azo coupling between 1-naphthol and diazotized sulfanilic acid. Bourne et al.[23] and Baldyga et al.[28] further extended the previous study and applied azo couplings between 1-naphthol and 2-naphthol with diazotized sulfanilic acid to the SMX® and SMXL® static mixers. Comparable results with the studies of Bourne and Maire[25] were reported. The more open structure of the SMXL® static mixer was found more attractive for fast reactions where high selectivity calls for rapid

Figure 2. Photographs of the pilot NETMIX® unit.

[Color figure can be viewed in the online issue, which is available at wileyonlinelibrary.com.]

mixing. Fang and Lee[29] quantitatively measured the micromixing efficiency of the Kenics® static mixer at Reynolds numbers ranging from $Re = 66$ to 1066 using the reaction scheme proposed by Villermaux and coworkers.[30,31] The static mixer was found to enhance micromixing efficiency in comparison with that in an empty tube. The results further revealed that the Kenics® static mixer could yield better degree of micromixing than a CSTR.

The results from this work have shown that the NETmix® technology is a new type of reactor where mixing can be controlled, particularly suited for complex, fast kinetics reactions, leading to the registration of an international patent, and now protected by an European patent.[32]

Experimental Setup

The prototype NETmix® unit, shown in Figure 2, is composed of a Plexiglas® static mixing device, the NETmix® static mixer, four independent feeding reservoirs, one discharging reservoir, two pump systems, and tubing with all the necessary fittings. The core of the unit is the NETmix® static mixer, and all accessory equipment serves the sole purpose of delivering fluid with precise flow rate control.

The NETmix® prototype structure is similar to the one modeled and studied previously,[4,5] with $n_x = 49$ rows of spherical chambers, connected by an oblique arrangement of cylindrical channels, each channel at an angle of $\phi = 45°$ with the main flow direction, the x axis. Each row alternates between 15 and 16 chambers, with the first row starting with 15 chambers. The number of columns is given by the maximum number of chambers in any row, and thus in this case $n_y = 16$.

Chambers in the first row are called inlet chambers, whereas the last-row chambers are referred as exit chambers (Figure 1). Each inlet and exit chamber includes two opposed channels, front and back, in the direction normal to the static mixer plane. This assembly results in a total of 30 inlet channels and 30 exit channels.

The characteristic dimensions of the chambers and channels are also in accordance with the ones used in the NETmix® model: chambers diameter $D = 7.0$ mm, channels diameter $d = 1.5$ mm, and oblique distance between two neighboring chamber centers $L^o = 10.0$ mm. These dimensions result in a total void volume of $V = 1.44 \times 10^{-4}$ m^3. The resulting value for the segregation parameter is $\alpha = 0.052$.

Inlet streams flow rates are controlled by two Ismatec® MCP Standard pump systems. Each pump system is capable of delivering from 3 to 750 ml/min per channel, and to develop a maximum differential pressure of 1.0 bar. To achieve the highest level of feeding control, a single pump system is used for the front inlet channels and the other pump system for the back inlet channels, ensuring an equal flow rate in all 15 inlet channels on each side.

Tracer Experiments

Visualization of tracer flow experiments allows a qualitative analysis of the NETMIX® mixing performance as a function of the Reynolds number. Macromixing can be studied through visualization of the steady-state overall patterns, and micromixing through local visualization of flow patterns, up to the smallest scale present, that corresponds to the behavior of individual static mixer chambers.

Tracer flow experiments were conducted for Reynolds numbers ranging from $Re = 25$ to 700, where $Re = \rho d v/\mu$, ρ and μ are the fluid density and viscosity, respectively, and v is the average velocity in the channels. Tap water was used as working fluid and methylene blue as the tracer.

Flow visualization of the experiments was done using TSI® imaging equipment consisting of a charge-coupled device (CCD) high-speed camera, a synchronizer, and a computer for image acquisition and components control. The control and data acquisition parameters were set using the graphical interface of the software Insight® from TSI®. The CCD camera is a PIVCAM 10-30 from TSI® with 1024 × 1024 pixels, each pixel with 8 bits definition, and a maximum frame rate of 30 Hz. The captured frames were transferred from the camera to the computer memory through a PCI card to be processed. To capture flow field images, the CCD camera must be triggered with the correct sequence and timing. The synchronizer performs this task, offering full computer control using an RS-232 interface, tying the CCD camera and PC computer together as an integrated and automated system.

Image acquisition is performed in the plane containing the chambers and channels centers, for which the geometry is similar to the NETmix® model, allowing an immediate and direct comparison with the model predictions.[4] Nearly uniform illumination and good light dispersion were obtained using a white photo reflector located between the static mixer and a halogen lamp.

Macromixing affects the spread of the material throughout the static mixer, and its assessment is done through the visualization of the tracer patterns at steady state. The tracer is injected on a single injector at the center column. Figure 3 shows snapshots of four tracer experiments for $Re = 37.5$, 50, 75, 150, 200, and 300, representative of the different possible behaviors.

For low Reynolds numbers ($Re = 25$), the tracer plume presents a 45° aperture in the first three rows, spreading to the neighboring two columns, but no further spread of tracer occurs up to the exit. This initial plume aperture most probably results from pump-induced perturbations in the flow, after which, outside the pump influence region, the plume keeps a uniform width. This behavior indicates that pump influence is restricted to the inlet neighboring region, being

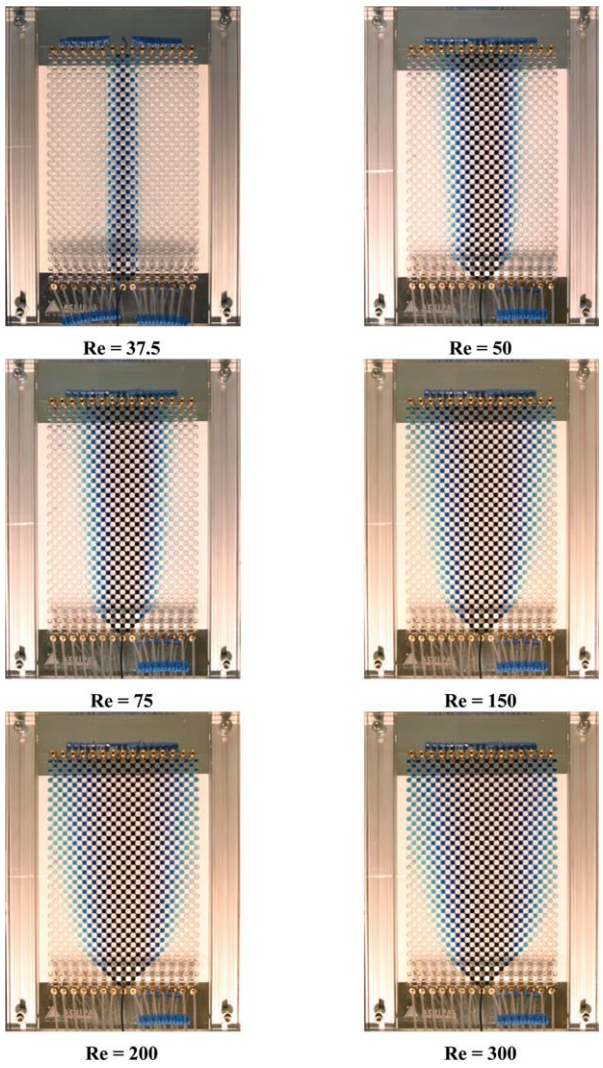

Figure 3. Snapshots of tracer experiments at steady state for a single central injection point.

[Color figure can be viewed in the online issue, which is available at wileyonlinelibrary.com.]

shortly dumped afterward. This quick dissipation of perturbation prevents the use of pulsed flow to overcome minimum Reynolds limits for mixing. The nonspreading of the plume is caused by a complete lack of mixing inside the chambers, i.e., each stream flows in its original entrance side of the chamber, completely segregated from the opposing stream.

Increasing the Reynolds number ($Re = 50$) the plume spreads to neighboring columns within the first four rows, but again no further spreading occurs up to the exit. At $Re = 75$, the plume starts to open continuously from the bottom to the top of the NETmix®, denoting a flow field transition with the onset of the occurrence of mixing mechanisms inside each chamber. For higher Reynolds numbers, a continuous increase in the plume aperture, up to the physical limit of 45°, can be observed. At $Re = 150$, the plume spreads across the whole width of the static mixer. For $Re \geq 200$, the overall tracer flow patterns become practically indistinguishable from each other.

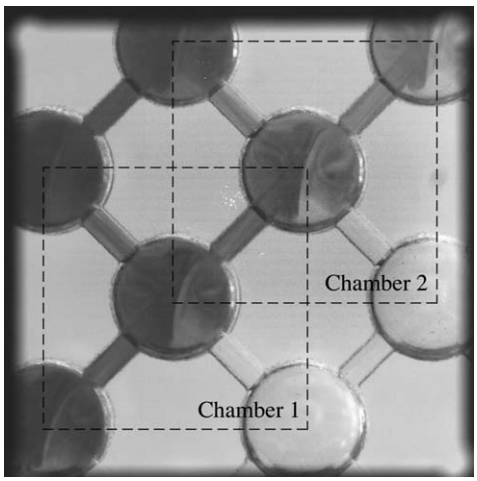

Figure 4. Typical digital frame obtained with the PIVCAM 10-30 camera for the tracer experiments.

Micromixing is associated with the homogenization of the mixture at the smallest scales. Thus, micromixing assessment is better achieved through the local visualization of mixing inside each chamber. The tracer forms an evolving plume from the single injection chamber toward the static mixer exit, as observed in Figure 3.

The mixing flow patterns are better observed in the chambers where clear and dyed fluid enter separately, thus the imaging acquisition frame was placed on the interface between dyed and clear streams and sufficiently distanced from the pumps influence region and static mixer borders. Figure 4 shows an example of one image frame acquired using the PIVCAM camera. Dynamic flow pattern sequences for two neighboring interface chambers were simultaneously acquired, allowing their comparison at the same time instant, for Reynolds numbers ranging from 37.5 to 500. At each flow condition and scanning position, an ensemble of 200 frames with a frequency of 30 Hz was captured. The scanned region is a square with side length of 25.2 mm and a resolution of 24.62 μm/pixel. This resolution allows the visualization of the smaller scales and an adequate imaging of the micromixing phenomena. To enhance mixing visualization, images were postprocessed by indexing each gray level to a color level ranging from white to blue.

Figure 5 shows some typical sequences of dynamic flow patterns in a single chamber. For low Reynolds numbers ($Re = 37.5$), nearly complete segregation between the two halves of the chamber is observed, denoting the total absence of convective transport between the dyed and clear streams. This particular flow pattern is the cause of no plume spreading toward the static mixer top observed for $Re < 50$ (see Figure 3). For $Re = 50$, the segregation between the two halves of the chamber is still observed, but now a slight oscillation is observed at the top of the chamber; this oscillation results in the slight plume spread shown in Figure 3 for $Re = 50$.

For $Re = 75$, a flow regime transition, with some degree of mixing between the two inlet streams, is observed. The separation between the two halves of the chamber is still observable, but now the tracer appears in the half where clear fluid is injected. Further analysis of the sequence of frames shows that the interface between the dyed and clear streams is continuously changing with time, and the flow field presents a self-sustained oscillatory behavior.

In the range $75 < Re \leq 200$, there is a clear increase in the mixing dynamics, where the amplitude of the interface oscillation grows with Re. Interface oscillation causes both streams to be constantly engulfed by the vortices structures located near the top and bottom wall of each chamber. Again a self-sustained oscillatory behavior is observed, and the time for a full oscillation decreases with Re.

The increase of the mixing dynamics makes the chamber homogenization nearly instantaneous, in particular for $Re > 200$ where the flow patterns become featureless. The quasi-instantaneous homogenization denotes very intensive mixing inside the chambers, which is next studied through the use of test reactions for micromixing characterization.

Although these experiments were conducted at constant flow rate, the flow visualization experiments put into

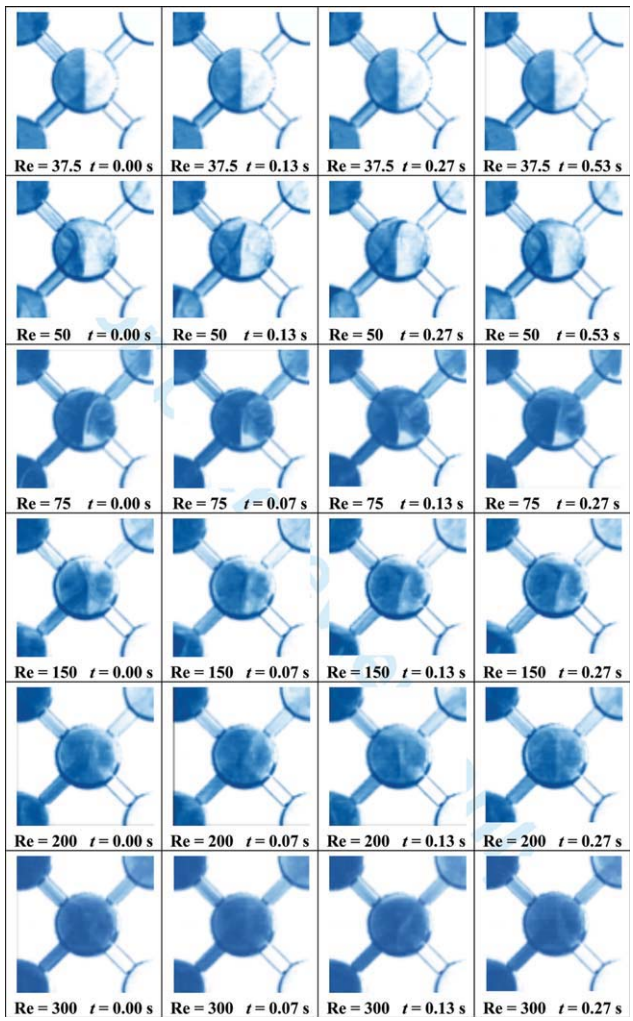

Figure 5. Single-chamber dynamic flow pattern sequences for tracer experiments.

[Color figure can be viewed in the online issue, which is available at wileyonlinelibrary.com.]

evidence the existence of flow field oscillation frequencies dependent of the Reynolds number. This oscillatory behavior was observed also in the case where only one pump was used, indicating that it is a phenomenon intrinsic to the flow field within the NETmix® structure and not induced by pump oscillations.

Chemical Reaction Experiments

Parallel and/or consecutive test reactions have been extensively used to study the mixing efficiency in chemical reactors, by exploiting the competition between two or more chemical reactions.[33–39] In this work, a consecutive/competitive reaction system, the azo coupling of 1-naphthol (A) with diazotized sulfanilic acid (B) in dilute, aqueous, and alkaline buffered solution was used for mixing studies. This reaction, first proposed by Bourne et al.,[40] is schematically represented by

$$\begin{aligned} A + B &\xrightarrow{k_1} R \quad \text{(very fast)} \\ R + B &\xrightarrow{k_2} S \quad \text{(fast)}, \end{aligned} \tag{1}$$

where R represents a mixture of the two isomers of the monoazo product: the ortho form, 2-(4′-sulphophenylazo)-1-naphthol, and the para form, 4-(4′-sulphophenylazo)-1-naphthol. S is the bisazo product: 2,4-bis(4′-sulphophenylazo)-1-naphthol. The reaction kinetics for this system in aqueous solution have been extensively studied,[41–43] and it has been shown that the resulting product selectivity is dependent on mixing.[41]

For this reaction system, the reactants are uncolored and the azo-coupling products present red coloring. Chemical reaction visualization experiments follow product formation inside the NETmix® reactor. The extent of the reaction zones allows the estimation of the local and global spatial product distribution as a function of the Reynolds number.

Mixing assessment was obtained by studying the selectivity of the azo coupling reaction and the influence of operating conditions, namely the reactants injection schemes on product formation. An important characteristic of the NETmix® technology is the capability of using different injection schemes by introducing the reactants into different inlet chambers. Figure 6 shows the different schemes used in this work. The first injection scheme (Figure 6a), with the two reactants A and B injected in two separate inlet chambers, was used for the visualization experiments. In the premixed injection scheme (Figure 6b), the two reactants are injected in alternate inlet chambers, resulting that, by the second row of the reactor, the two reactants are fully mixed. In the three segregated injection schemes, reactant B is injected into one, two, and three inlet chambers, in a centrally symmetric pattern, with reactant A being injected in all the other inlet chambers (Figures 6c–e).

Visualizing chemical reaction at the local level can be used to assess the role of the flow field on micromixing, as the products formation only occurs when reactants contact at the molecular level. In addition, chemical reaction allows a clearer picture of the interaction between both inlet streams, in each chamber, as colored products are only formed in the contact regions.

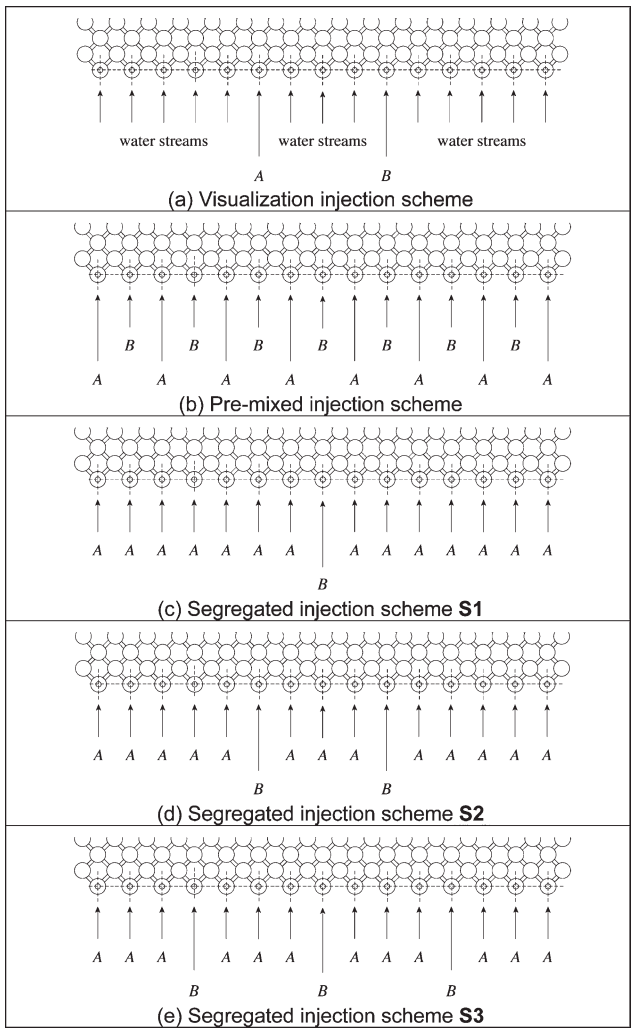

Figure 6. Chemical reaction experiments injection schemes.

The location of the injection points was set in such a way that the contact between the two reactants first occurs in a chamber positioned after the pumps influence region. To this purpose, reactants A and B are injected into two separate inlet chambers separated by three other inlet chambers as shown in Figure 6a, and thus the contacting chamber is located in the fourth row from the inlet.

Chemical reaction visualization experiments were conducted at steady state, for Reynolds numbers in the range of $50 \leq Re \leq 700$. Below $Re < 50$, the lack of mixing inside the chambers, as observed in the tracer experiments, keeps reactants A and B segregated from each other.

Figure 7 shows snapshots of the chemical reaction experiments for four typical values of Re. The azo couplings reaction products R and S all present an intense red color, but the S product color is noticeably darker. As in the tracer experiments, an increase of the plume aperture with higher Reynolds numbers is also observed here, but now color gradients within the plume are observed in both the main flow direction and in the direction normal to the flow. This effect results from the axis-symmetric spatial distributions of the reaction products R and S.

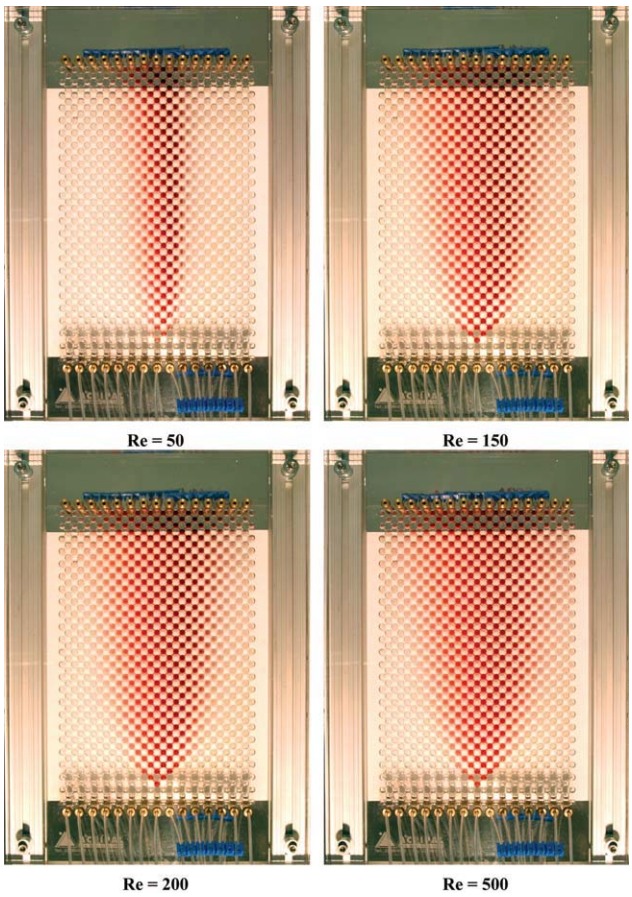

Figure 7. Snapshots of chemical reaction experiments at steady state using the visualization injection scheme (Figure 6a).

[Color figure can be viewed in the online issue, which is available at wileyonlinelibrary.com.]

As the reactants A and B are injected separately, a concentration gradient for each chemical species occurs along the direction normal to the flow. On the left-hand side of the reactor, A is predominant and thus all B is immediately consumed into R with only residual quantities of S being possibly formed, and thus the lighter red color observed. Conversely, on the right-hand side of the reactor, B is in excess, and a considerable quantity of B remains unreacted even after complete consumption of A into R, thus promoting the production of S, resulting in a darker red color.

The increase in mixing with Reynolds number flattens the reactants concentration gradients, thus notoriously affecting the product distribution. On the left-hand side, as Re increases, the reduced but still present excess of A always results in a complete consumption of B into R, thus no visible coloring change occurs on that side of the plume. However, on the right-hand side, as the excess of reactant B relative to A diminishes for higher Re, the formation of product S is prevented, thus the fading of the dark red color on the right side of the plume, resulting in more homogeneous red color across the reactor.

From the tracer experiments results, an increasingly larger spatial spread of reactants with Re was expected. However, the continuous decrease of S formation in certain spatial locations as the Reynolds number increases is not only evidence of the increasingly greater spread of reactants A and B through the reactor, i.e., macromixing, but also the increasingly reduction of local segregation, i.e., micromixing. Hence, these experiments clearly show an overall increase of mixing, both macromixing and micromixing, with Re.

To further observe the effects of mixing on chemical reaction, dynamic imaging sequences of chemical reaction in a single chamber were obtained, choosing the chamber where both pure reactants A and B first contact. For each flow condition, an ensemble of 200 frames was captured with a frequency of 30 Hz. Again, to enhance the visualization, images were postprocessed, now indexing each gray level to a color level ranging from white to red.

From the complete dynamic sequences, obtained for Reynolds numbers in the range $50 \leq Re \leq 700$, a snapshot at a given time instant is shown in Figure 8. For $Re = 50$, product formation is restricted to the chamber central region, and mixing is insufficient to promote homogeneity of both reactant streams separately entering the chamber. A strong red color is only observable on the right-hand side exit chamber, resulting from the formation of S driven by the excess of B on this side of the reactor. For $Re = 75$, product formation on the whole chamber can be observed, even though the right-hand side exit chamber still presents a noticeably darker color. Although mixing was greatly improved, as observed from the chamber's homogeneous appearance, in micromixing terms an excess of B on the right side of the chamber still exists resulting in considerable more S formation. For $Re = 100$, no significant mixing quality enhancement is observed, but for $Re = 150$, it is observed a blurring between the red color intensities of both the left- and right-hand side exit chambers. For $Re \geq 200$, no further improvements in mixing are observable, either for micromixing or macromixing.

The reaction rates of the fast consecutive competitive reaction system described by Eq. 1 are high relative to the rate at which the reactants A and B are mixed. Thus, the azo coupling reaction product distribution strongly depends upon the mixing intensity, and the reaction selectivity becomes a suitable parameter for characterizing mixing.

The maximum selectivity value in R is obtained when the contact of A and B at the molecular level scale is done before significant reaction occurs; otherwise, if homogenization is slow, the selectivity values tend to zero. The selectivity in S is given by[44]

$$X_S = \frac{2C_S^{\text{out}}}{C_R^{\text{out}} + 2C_S^{\text{out}}}, \tag{2}$$

where C_R^{exit} and C_S^{exit} are the products exit concentrations.

When reaction is sufficiently slow that its rate is determined by chemical kinetics, the reactants streams can be mixed before any significant conversion occurs, and micromixing is not important in these cases.[45] When reaction is fast relative to mixing, conversion occurs in reaction zones where steep concentration gradients are present, which has influence in product distribution.[35] In the azo coupling of 1-naphthol (A) with diazotized sulfanilic acid (B), the couplings are so fast that reaction is complete within a few

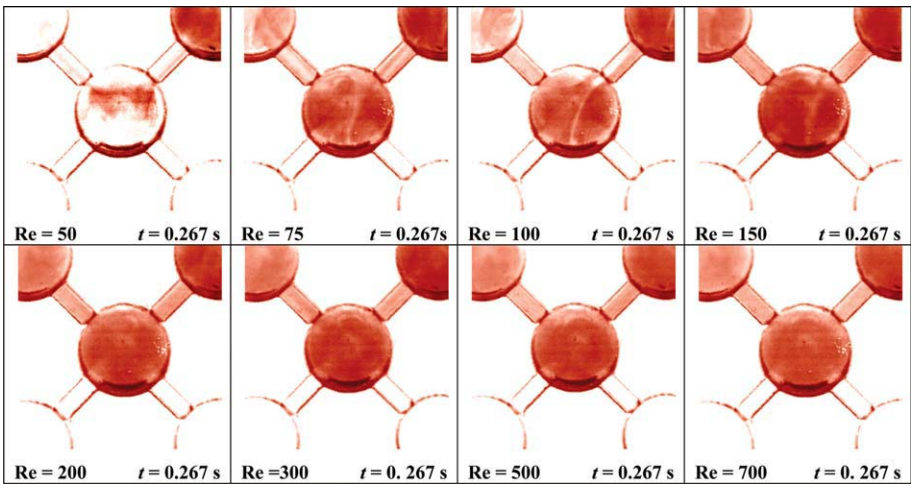

Figure 8. Single-chamber dynamic flow patterns for chemical reaction experiments.

[Color figure can be viewed in the online issue, which is available at wileyonlinelibrary.com.]

seconds. Thus, A and B were, for all experiments, separately fed into the NETmix® to assess mixing only within the reactor, avoiding external premixing effects that would distort the results and their meaning. Preparation of the reactants followed a strict procedure[5,43] to ensure their stabilization and an optimum value of pH around 10.

Product distribution at the reactor exit was determined by spectrophotometry using a stopped-flow reaction technique.[5,43] To obtain significant quantities of R, and thus simplify their determination, the inlet reactant concentration ratio, C_A^{in}/C_B^{in}, should be higher than the stoichiometric ratio. However, ratios greatly in excess of unity cause low S formation and again analytical problems.[40] In this work, a ratio of $C_A^{in}/C_B^{in} = 1.2$ was used for all azo couplings. Furthermore, as A is always in excess, reactant B becomes the limiting reactant, thus enabling a way of verifying the overall mass balance.

$$C_B^{exit} = C_B^{in} + C_R^{exit} + 2C_S^{exit}. \quad (3)$$

Two types of experiments were conducted. First, a premixed injection scheme (Figure 6b) was used to promote early mixing and maximize the reactants feed distribution.[45] This premixed injection scheme accelerates mixing, establishing in this way a high selectivity in R (lower X_S) for given hydrodynamic operating conditions. Furthermore, it provides a straightforward approach for mixing assessment at different values of Re.

The second type of experiments takes advantage of the various inlets of the NETmix® reactors, where reactants are fed with different, segregated injection schemes (Figures 6c, d). This study aims to find ways of controlling product distribution, for given hydrodynamic operating conditions. Similar works have been conducted to study the effect of the number of feed nozzles of reactant B on the selectivity of S in stirred tanks.[46]

The reactants were fed, and all the experiments were carried out at 20°C. All inlet ports were fed with feed concentrations, C_A^f and C_B^f, determined so that for all schemes the overall inlet concentration rate is equal to $C_A^{in}/C_B^{in} = 1.2$ (Table 1). For both premixed and segregated injection schemes, and at every Reynolds numbers studied, samples were collected from all exit channels of the reactor. Each sample was immediately analyzed twice to ensure the spectrophotometric method reproducibility and to verify if chemical reaction only occurs inside the reactor.

For the premixed injection scheme, given that no concentration profile at the exit channels occurs, values of C_R^{exit} and C_S^{exit} were evaluated as arithmetic averages of all the measured concentrations values in each experiment, for each Reynolds number. In all experiments, the conversion of the limiting reactant B was complete, and the mass balance (Eq. 1) for the two products, R and S, was between 98 and 100% of the amount B added to the reactor.

Figure 9 shows, for the premixed injection scheme, plots of the products concentration at the reactor exit and of the selectivity X_S where it is clear the major effect of the Reynolds number on macromixing and micromixing. From $Re =$ 50 to 250, the amount of S produced decreases rapidly, and

Table 1. Feed Concentrations of Reactants *A* and *B* Concentrations for Each Injection Reaction Scheme

Injection Scheme	Feed Concentrations (Before Mixing) (mol m^{-3})	Feed Concentrations (After Mixing) (mol m^{-3})
Prémixed injection scheme	$C_A^f = 0.450$ $C_B^f = 0.429$	$C_A^{in} = 0.300$ $C_B^{in} = 1.000$
Segregated injection scheme S1	$C_A^f = 0.257$ $C_B^f = 3.000$	
Segregated injection scheme S2	$C_A^f = 0.277$ $C_B^f = 1.500$	
Segregated injection scheme S3	$C_A^f = 0.300$ $C_B^f = 1.000$	

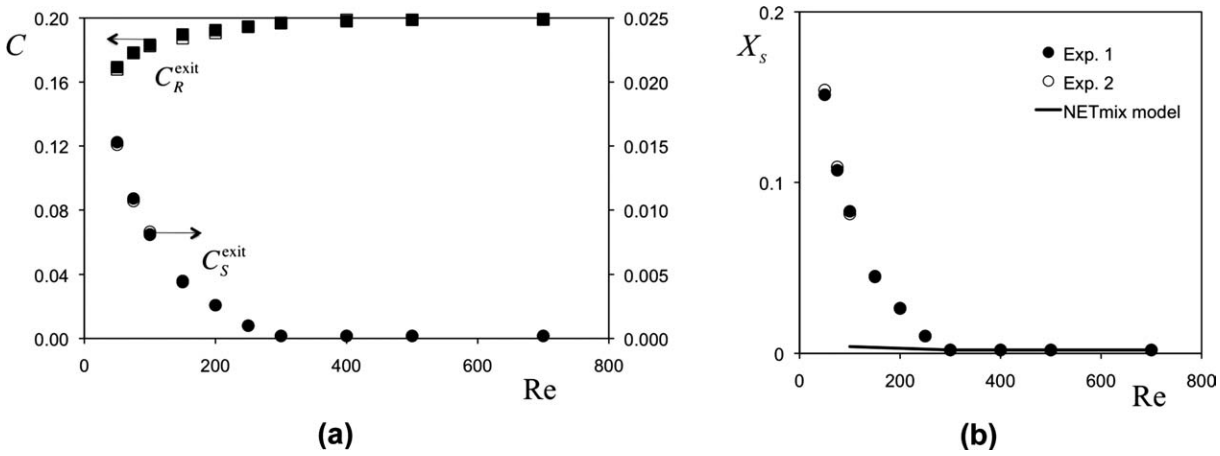

Figure 9. Results obtained for the premixed injection scheme as a function of the Reynolds number.

(a) Exit product concentration and (b) selectivity in *S*.

X_S reaches an asymptotic value of nearly zero for $Re \geq 300$. In terms of either macromixing or micromixing, this indicates a severe increase in the mixing intensity in the range $50 \leq Re \leq 250$, and that for $Re \geq 300$ the product distribution is no longer in a macromixing- or micromixing-controlled regime.

Experiments were also conducted for the three different segregated injection schemes shown in Figures 6c, d, where reactant *B* is injected in one, two, and three zones. Similarly to the premixed injection scheme experiments, concentration evolution with time was not observed in these experiments. In these cases, the limiting reactant *B* is not completely consumed inside the reactor, except for the case of segregated injection scheme S3. Again the mass balance to *B* was within 98–100.0% for both *Re*.

Figure 10 shows values of X_S determined in the exit channels of reactor, for the three segregated injection schemes and $Re = 300$ and 500. The profiles of X_S, along the exit channels, exhibit central symmetry, and for a given Reynolds number, the reactants injection scheme strongly affects the selectivity in *S*, with X_S markedly decreasing as the number of reactant *B* injection zones increases. The comparison of the profiles of X_S for the same segregated injection scheme at $Re = 300$ and 500 reveals similar spatial distributions, but lower selectivity in *S* as the Reynolds number increases. For the segregated injection schemes S1 and S2, a maximum value of X_S located at the central exit channel of the NETmix® is observed. As the number of injection zones increases, for both *Re*, a flattening of the X_S profile of along the exit channels of the reactor is observed, with a nearly flat profile for segregated injection scheme S3. Although flat profiles of X_S were also obtained along the exit channels for the premixed injection scheme, the average selectivity values for the segregated injection scheme S3, $X_S = 0.017$ and 0.085 for $Re = 300$ and 500, respectively, are one order of magnitude larger than the corresponding selectivity values for the premixed injection scheme, $X_S \approx 0.002$. Therefore, the product distribution for the present reaction scheme is shown to be dependent on the details of mixing-reaction interactions.

Comparison with the NETmix® Model

In a previous publication,[4] the NETmix® model was introduced, where macromixing modeling is based on the network structure and on the assumptions of perfectly mixed chambers and piston flow in the channels. The hydrodynamics is simulated using an analogy to a pure resistive electrical circuit with no dependency on the Reynolds number.[47]

To further validate the NETmix® model, simulations were carried out using a regular network with nonperiodic boundary conditions and without horizontal channels,[4] with the same dimensions as the NETmix® static mixer prototype, and the results were compared with the experimental results.

The tracer snapshots of Figure 3 show a continuously evolving tracer spread for Reynolds numbers ranging from $Re = 25$ to 200, whereas for $Re \geq 300$, the tracer plume aperture attains the limit of 45°, with any further evolution in the overall tracer patterns virtually impossible to differentiate. Figure 11 compares the simulated and observed spread of tracer in the NETmix® model and prototype for a single central injection point. For Figure 11a, a color scale based on the simulated concentration maps was generated to

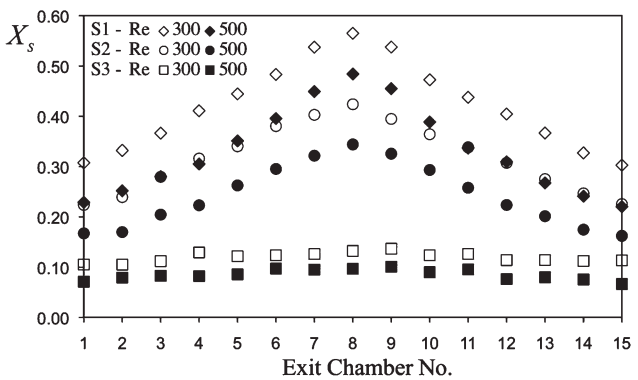

Figure 10. Selectivity in *S* at each outlet channel for different segregated injection schemes at *Re* = 300 and 500.

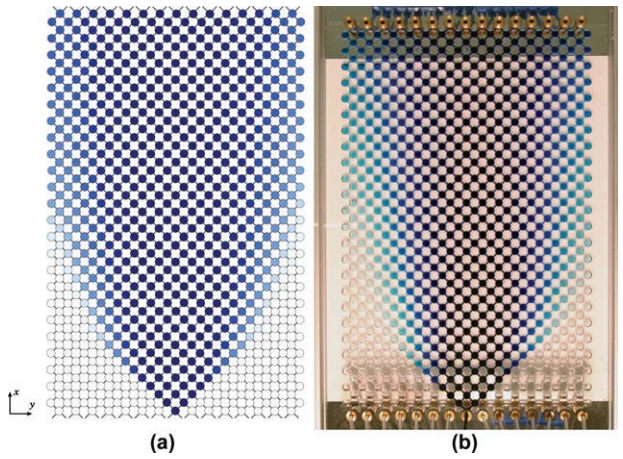

Figure 11. Tracer patterns for a single central injection point.

(a) NETmix® model simulation; (b) snapshot of tracer experiment at steady state for $Re = 500$. [Color figure can be viewed in the online issue, which is available at wileyonlinelibrary.com.]

approach the successive dilution of the methylene blue solution used in the tracer experiments.

To interpret the mixing-reaction experiments and compare with the NETmix® model data, it is important to have reliable chemical kinetic information. Different authors[36,40–42,48,49] have reported results of stopped-flow kinetic experiments for the set of reactions described by Eq. 1. Nonetheless the range of published values for rate constants, all works report both azo coupling reactions to be irreversible and second order in concentration dependence so that

$$\begin{aligned} -r_A &= k_1 C_A C_B \\ r_S &= k_2 C_B C_R. \end{aligned} \tag{4}$$

Nunes et al.[42,43] reported $k_1 = 15.8 \times 10^3$ m^3 mol^{-1} s^{-1} and $k_2 = 2.7$ m^3 mol^{-1} s^{-1} at pH = 9.9 and $T = 20$°C, obtained in a SX.18MV-R Microvolume Stopped-Flow Reaction Analyzer, and these values were used in all simulations.

The full line shown in Figure 9b represents the simulated values of the selectivity in S for the premixed injection scheme. For $Re \geq 300$, the NETmix® model describes accurately the experimental results, thus providing strong evidence that, in these cases, mixing is well described by the NETmix® model.

Figure 12 shows the experimental and simulated concentrations of reactant B and products R and S profiles at each exit channel and $Re = 300$. Very good agreement is obtained between the experiments and NETmix® model predictions, thus validating the assumptions that for high Reynolds numbers, channels behave as PFRs and chambers behave as perfectly mixed CSTRs, exhibiting no hydrodynamic or mixing dependency on the Reynolds number.

The validation of the NETmix® model as a macromixing, micromixing, and chemical reaction descriptive model of the NETmix® static mixer allows the estimation of concentration maps inside the reactor directly from simulations results. As an example, the computed concentration field maps of reactant B and products R and S for $Re = 300$ are shown in Figure 13 for the segregated injection scheme S2.

The distribution of R and S within the reactor is shown to be dependent on the details of the reactants A and B spatial distributions. Higher concentrations of R occur in the contact region between reactants A and B, with regions rich in R delimiting the B-rich regions. When spatial inhomogeneity of A and B concentrations occur, excess of B in the presence of A yields R that is later consumed into S. This is clearly the case, with the local maximum regions of B overlapping for the three segregated injection schemes with local deficit regions of R. Such general behavior for the case of a fast consecutive competitive reaction system was noted and qualitatively discussed by Levenspiel[2] and Bourne and Toor,[50]

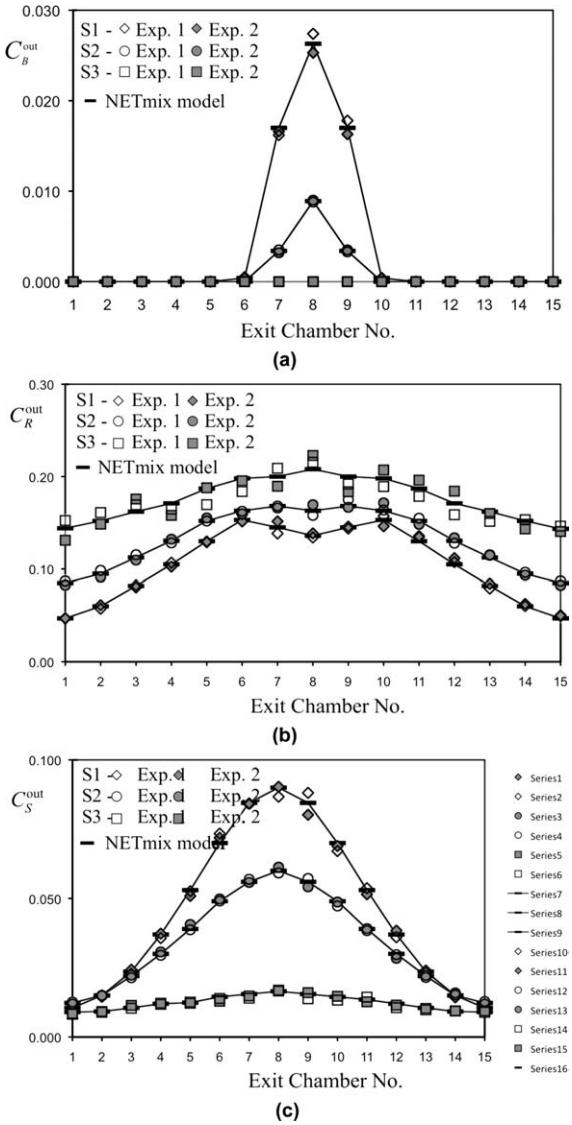

Figure 12. Simulated and experimental concentrations at the exit channels for *Re* = 300.

(a) reactant B; (b) product R; and (c) product S.

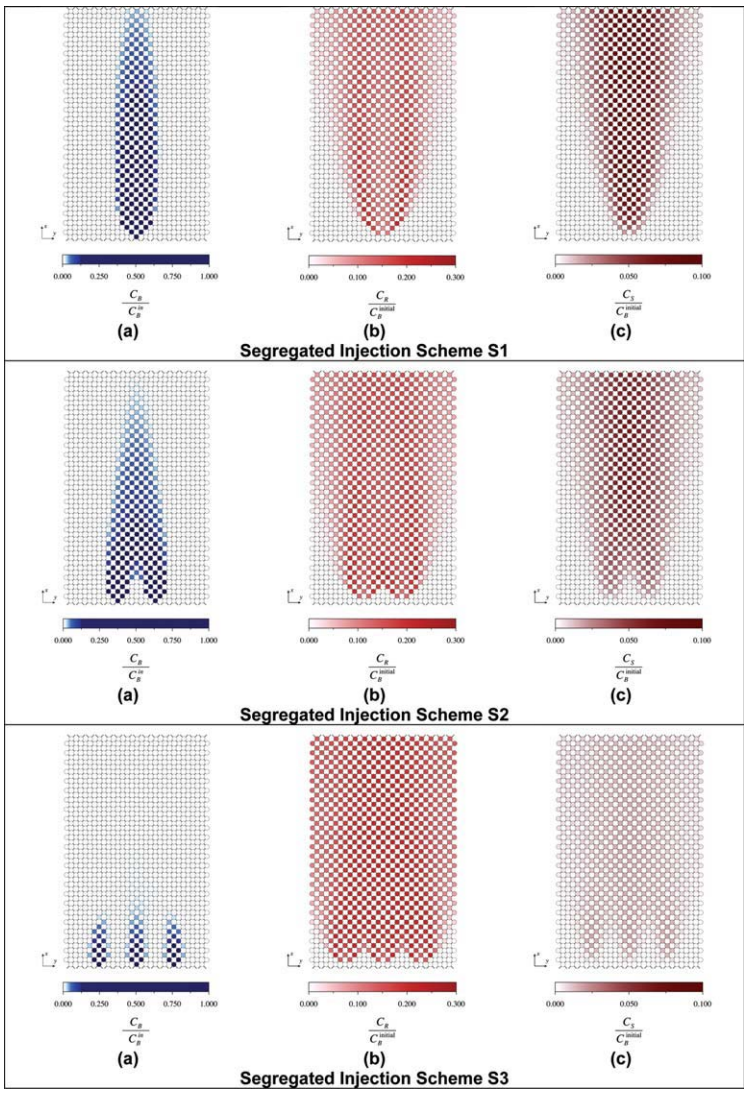

Figure 13. Simulated concentration field maps for *Re* = 300.

(a) reactant *B*; (b) product *R*; and (c) product *S*. [Color figure can be viewed in the online issue, which is available at wileyonlinelibrary.com.]

with subsequent experimental studies[51,52] and DNS simulations confirming the general validity of this observation.[53]

The experimental selectivity in *S* profiles, shown in Figure 10, presents maximum values at the central exit channel. Such feature is implicit in Figure 13, noticing that contact between reactants *A* and *B* is not sufficient to completely consume *B* in the NETmix® center axis, thus resulting in high formation of *S* in that region. On the other hand, the local maximum of *B* in the center axis promotes the consumption of *R*, resulting in the local minimum of *R* observed in Figure 10b.

Using different reactants injection schemes is shown here to be a key factor to control and attain different product selectivity values. As fast consecutive competitive reactions offer a stringent test of reactive mixing, the ability of the NETmix® model to handle and describe different situations, such as the use of segregated injection schemes, results in its validation as a tool for product distribution design.

Conclusions

The NETmix® static mixer mixing efficiency was assessed through tracer flow visualization experiments in the range of Reynolds numbers $25 \leq Re \leq 700$. The importance of the work presented lies in the fact that it contributes to the knowledge of the influence of the operating *Re* in the NETmix® static mixer dynamic behavior. It is clear the existence of a transition in the flow field regime for a critical Reynolds number around 75, with the onset of mixing mechanisms inside each chamber. For $Re < 75$, an almost complete segregation between the fluids in the two halves of the chamber is observed. Above the critical Reynolds number, a continuous increase in the mixing dynamics is observed, with quasi-instantaneous chamber homogenization achieved for $Re \geq 200$.

A good match between the NETmix® model[4,5] and the NETmix® static mixer macromixing patterns was shown from tracer flow visualization experiments, validating the

NETmix® model as a macromixing descriptive model for $Re \geq 300$.

Greater insight into the mixing efficiency of the NETmix® static mixer was achieved through chemical reactions experiments using as test reaction a fast consecutive competitive reaction system, the azo coupling of 1-naphthol with diazotized sulfanilic acid. As the azo coupling reaction product distribution strongly depends upon the mixing intensity, the selectivity in S can be used to further assess the NETmix® model validity for mixing and reaction. Chemical reaction imaging provided further evidence on the overall increase of mixing, both macromixing and micromixing, with Re.

Experiments to determine the product distribution at the exit channels NETmix® static mixer were carried out for different Reynolds numbers and reactants injection schemes. Under the premixed injection scheme, the selectivity in S strongly decreases in the range of Reynolds numbers $50 \leq Re \leq 250$, displaying nearly zero values for $Re \geq 300$. This indicates a severe increase in mixing intensity up to $Re = 300$, with the product distribution being no longer in a macromixing- or micromixing-controlled regime for higher Reynolds numbers. Similar to the results for macromixing, an excellent fit of mixing-reaction experimental data was obtained with the NETmix® model for $Re \geq 300$.

NETmix® model simulations showed a strong product distribution dependency on the reactants injection scheme. The feasibility of using segregated injection schemes as an operational and design parameter in the NETmix® static mixer was experimentally shown for $Re = 300$ and 500. Agreement between experiments and predictions was excellent for both Reynolds numbers, thus supporting for the NETmix® static mixer the assumptions of the NETmix® model that channels behave as PFRs and chambers behave as perfectly mixed CSTRs for $Re \geq 300$.

The agreement between chemical reaction experimental data and NETmix® model predictions with segregated injection schemes provides a firm basis to its ultimate assertion as a macromixing and micromixing and chemical reaction descriptive model for the NETmix® static mixer, under the appropriate conditions.

Moreover, the NETmix® technology, now protected by an European patent,[32] has proven to be an innovative type of reactor where mixing can be controlled particularly suited for complex, fast kinetics reactions. Because of its 2D configuration, it is a versatile technology, of easy scale-up, with high heat transfer area required in highly exothermic and explosive reactions. The NETmix® has been used in a new, proprietary[54] continuous process for production of highly pure, nanocrystalline hydroxyapatite using a wet chemical method of precipitation using calcium and phosphorus in alkaline solution.[55]

Acknowledgments

Financial support for this work was in part provided by national research grant FCT/POCTI/EQU/34151/99 for which the authors are thankful. P.E. Laranjeira, A.A. Martins, and M.I. Nunes acknowledge their Ph.D. scholarships by FCT, PRAXIS XXI/BD/21490/99, PRAXIS XXI/BD/2631/93, and PRAXIS XXI/BD/9296/96, respectively.

Literature Cited

1. Ottino JM. Mixing and chemical reactions: a tutorial. *Chem Eng Sci*. 1994;49:4005–4027.
2. Levenspiel O. *Chemical Reaction Engineering*. New York: Wiley, 1972.
3. Zalc JM, Muzzio FJ. Parallel-competitive reactions in a two-dimensional chaotic flow. *Chem Eng Sci*. 1999;54:1053–1069.
4. Laranjeira PE, Martins AA, Lopes JCB, Dias MM. NETmix®, a new type of static mixer: modeling, simulation, macromixing, and micromixing characterization. *AIChE J*. 2009;5:2226–2243.
5. Laranjeira PEMSC. NETMIX® static mixer—modelling, CFD and experimental characterization, PhD thesis. Porto: Faculdade de Engenharia da Universidade do Porto, 2006.
6. Lanning LM, Ford RM. Glass micromodel study of bacterial dispersion in spatially periodic porous networks. *Biotechnol Bioeng*. 2004;78:556–566.
7. Corapcioglu MY, Ferdirchuck P. Glass bead micromodel study of solute transport. *J Contam Hydrol*. 1999;36:209–230.
8. Willingham TW, Werth CJ, Valocchi AJ. Evaluation of the effects of porous media structure and mixing-controlled reactions using pore-scale modeling and micromodel experiments. *Environ Sci Technol*. 2008;42:3185–3193.
9. Jia C, Shing K, Yortsos YC. Visualization and simulation of non-aqueous phase liquids solubilization in pore networks. *J Contam Hydrol*. 1999;35:363–387.
10. Shaloul NA, Ioannidis MA, Chatzis I. Dissulotion of residual non-aqueous phase liquids in porous media: pore-scale mechanisms and mass transfer rates. *Adv Water Res*. 2002;25:33–49.
11. Jeong SW, Corapcioglu MY. A micromodel analysis of factors influencing NAPL removal by surfactant foam flooding. *J Contam Hydrol*. 2003;60:77–96.
12. Theodoropoulu MA. Dispersion of dissolved contaminants in groundwater: from visualization experiments to macroscopic simulation. *Water Air Soil Pollut*. 2007;181:235–245.
13. Kim DS, Fogler HS. Biomass evolution in porous media and its effects on permeability under starvation conditions. *Biotechnol Bioeng*. 2000;69:47–56.
14. Stewart T, Fogler HS. Biomass plug development and propagation in porous media. *Biotechnol Bioeng*. 2001;72:353–363.
15. Dunsmore BC, Bass CJ, Lappin-Scott HM. A novel approach to investigate biofilm accumulation and bacterial transport in porous matrices. *Environ Microbiol*. 2004;6:183–187.
16. Hinkley RE, Dias MM, Payatakes AC. On the motion of oil ganglia in porous media. *Physicochem Hydrodyn*. 1987;8:185–211.
17. Dominguez A, Bories S, Prat M. Gas cluster growth by solute diffusion in porous media. Experiments and automaton simulation on pore networks. *Int J Multiphase Flow*. 2000;26:1951–1979.
18. Perrin CL, Tardy PMJ, Sorbie KS, Crawshaw JC. Experimental and modeling study of newtonian and non-newtonian fluid flow in pore network micromodels. *J Colloid Interface Sci*. 2006;295:542–550.
19. Zerai B, Saylor BZ, Kadambi JR, Oliver MJ, Mazaheri AR, Ahmadi G, Bromhal GS, Smith DH. Flow characterization through a network cell using particle image velocimetry. *Transport Porous Media*. 2005;60:159–181.
20. Dertinger SKW, Chiu DT, Jeon NL, Whitesides GM. Generation of gradients having complex shapes using microfluidic networks. *Anal Chem*. 2001;73:1240–1246.
21. Baldyga J, Bourne JR. *Turbulent Mixing and Chemical Reactions*. New York: Wiley, 1999.
22. Bourne JR. Mixing and the selectivity of chemical reactions. *Org Process Res Dev*. 2003;7:741–508.
23. Bourne JR, Lenzner J, Petrozzi S. Micromixing in static mixers: an experimental study. *Ind Eng Chem Res*. 1992;31:1216–1222.
24. Meyer T, David R, Renken A, Villermaux J. Micromixing in a static mixer and an empty tube by a chemical method. *Chem Eng Sci*. 1988;43:1955–1960.
25. Bourne JR, Maire H. Micromixing and fast chemical reactions in static mixers. *Chem Eng Process*. 1991;30:23–30.
26. Baldyga J, Bourne JR. Simplification of micromixing calculations. I. Derivation and application of new model. *Chem Eng J*. 1989;42:83–92.
27. Baldyga J, Bourne JR. Simplification of micromixing calculations. II. New applications. *Chem Eng J*. 1989;42:93–101.
28. Baldyga J, Bourne JR, Hearn SJ. Interaction between chemical reactions and mixing on various scales. *Chem Eng Sci*. 1997;52:457–466.
29. Fang JZ, Lee DJ. Micromixing efficiency in static mixer. *Chem Eng Sci*. 2001;56:3797–3802.

30. Villermaux J, Falk L, Fournier MC. Potential use of a new parallel reaction system to characterise micromixing in stirred reactors. *AIChE Symp Ser*. 1994;90:50–54.
31. Fournier MC, Falk L, Villermaux J. A new parallel competing reaction system for assessing micromixing efficiency—experimental approach. *Chem Eng Sci*. 1996;53:5053–5064.
32. Lopes JCB, Laranjeira PE, Dias MMGQ, Martins AA. Network mixer and related mixing process. PCT/IB2005/000647, February 2005. Eur Pat. EP172643 B1, October 2008.
33. Bourne JR, Kozicki F. Mixing effects during the bromination of 1,3,5-trimethoxybenzene. *Chem Eng Sci*. 1977;32:1538–1539.
34. Bourne JR. The characterization of micromixing using fast multiple reactions. *Chem Eng Commun*. 1982;16:79–90.
35. Bourne JR, Oemer MK, Lenzner J, Maire H. Kinetics of the diazo coupling between 1-naftol and diazotized sulfanilic acid. *Ind Eng Chem Res*. 1990;29:1761–1765.
36. Villermaux J, Falk L, Fournier MC, Detrez C. Use of parallel competing reactions to characterize micromixing efficiency. *AIChE Symp Ser*. 1992;88:6–10.
37. Bourne JR, Yu S. Investigation of mircomixing in stirred tank reactors using parallel reactions. *Ind Eng Chem Res*. 1994;33:41–55.
38. El-Hamouz AM, Mann R. Effect of micro-mixing on the yield of intermediates in triplet consecutive/competitive reactions. *Can J Chem Eng*. 1998;76:650–656.
39. Bourne JR, Kozicki F, Rys P. Mixing and fast chemical reaction. I. Test reactions to determine segregation. *Chem Eng Sci*. 1981;36:1643–1648.
40. Bourne JR, Kut OM, Lenzner J. An improved reaction system to investigate micromixing in high-intensity mixers. *Ind Eng Chem Res*. 1992;31:949–958.
41. Bourne JR. Mixing on the molecular scale (micromixing). *Chem Eng Sci*. 1983;38:5–8.
42. Nunes MI, Dias MM, Lopes JCB. Kinetic study of fast reactions in viscous media. Paper Presented at the CHEMPOR'2001, Aveiro, Portugal, 2001.
43. Nunes MI. Micromixing in chemical reactors—test reactions. PhD thesis. Porto: Faculdade de Engenharia da Universidade do Porto, 2008.
44. Bourne JR, Schwarz G, Sharma RN. A new method for studying diffusive mixing in a tubular reactor. *Paper Presented at the 4th European Conference on Mixing*, Cranfield, England, 1982.
45. Angst W, Bourne JR, Sharma RN. Mixing and fast chemical reaction. IV. The dimensions of the reaction zone. *Chem Eng Sci*. 1982;37:585–590.
46. Bourne JR, Hilber CP. The productivity of micromixing-controlled reactions: effect of feed distribution in stirred tanks. *Chem Eng Res Des*. 1990;68:51–56.
47. Martins AA, Laranjeira PE, Lopes JCB, Dias MM. Network modelling of flow in a packed bed. *AIChE J*. 2007;53:91–107.
48. Bourne JR, Hilbert C, Tovstiga G. Kinetics of the azo coupling reactions between 1-naftol and diazotized sulfanilic acid. *Chem Eng Commun*. 1985;37:293–314.
49. Wenger KS, Dunlop EH, MacGilp ID. Investigation of the chemistry of a diazo micromixing test reaction. *AIChE J*. 1992;38:1105–1114.
50. Bourne R, Toor HL. Simple criteria for mixing effects in complex reactions. *AIChE J*. 1977;23:602–604.
51. Paul EL, Treybal RE. Mixing and product distribution for a liquid-phase, second-order, competitive-consecutive reaction. *AIChE J*. 1971; 17:718–724.
52. Bourne JR, Kozicki F, Moergeli U, Rys P. Mixing and fast chemical reaction. III. Model-experiment comparisons. *Chem Eng Sci*. 1981;36:1655–1663.
53. Chakrabarti M, Kerr RM, Hill JC. Direct numerical simulation of chemical selectivity in homogenous turbulence. *AIChE J*. 1995;41: 2356–2370.
54. Lopes JCB, Dias MMGQ, Silva VMTM, Santos PAQO, Monteiro FJM, Gomes PJC, Mateus AYP. Production method for calcium phosphate nano-particles with high purity and their use. PCT/PT2007/000031, July 2007.
55. Gomes PJ, Silva VMTM, Quadros PA, Dias MM, Lopes JCN. A highly reproducible continuous process for hydroxyapatite nanoparticles synthesis. *J Nanosci Nanotechnol*. 2009;9:3387–3395.

Manuscript received Nov. 16, 2009, and final revision received May 24, 2010.